actuators

MDPI

Article

Disturbance Observer-Based Backstepping Control of Tail-Sitter UAVs

Nihal Dalwadi [1,†], Dipankar Deb [1,*,†], Mangal Kothari [2,†] and Stepan Ozana [3,†]

[1] Department of Electrical Engineering, Institute of Infrastructure Technology Research and Management (IITRAM), Ahmedabad 380026, India; nihal.dalwadi.20pe@iitram.ac.in
[2] Department of Aerospace Engineering, Indian Institute of Technology, Kanpur 380026, India; mangal@iitk.ac.in
[3] Department of Cybernetics and Biomedical Engineering, Faculty of Electrical Engineering and Computer Science, VSB-Technical University of Ostrava, 17. listopadu 2172/15, 708 00 Ostrava-Poruba, Czech Republic; stepan.ozana@vsb.cz
* Correspondence: dipankardeb@iitram.ac.in
† These authors contributed equally to this work.

Abstract: The application scope of unmanned aerial vehicles (UAVs) is increasing along with commensurate advancements in performance. The hybrid quadrotor vertical takeoff and landing (VTOL) UAV has the benefits of both rotary-wing aircraft and fixed-wing aircraft. However, the vehicle requires a robust controller for takeoff, landing, transition, and hovering modes because the aerodynamic parameters differ in those modes. We consider a nonlinear observer-based backstepping controller in the control design and provide stability analysis for handling parameter variations and external disturbances. We carry out simulations in MATLAB Simulink which show that the nonlinear observer contributes more to robustness and overall closed-loop stability, considering external disturbances in takeoff, hovering and landing phases. The backstepping controller is capable of decent trajectory-tracking during the transition from hovering to level flight and vice versa with nominal altitude drop.

Keywords: quadrotor tail-sitter UAV; nonlinear observer; backstepping control; trajectory-tracking

check for updates

Citation: Dalwadi, N.; Deb, D.; Kothari, M.; Ozana, S. Disturbance Observer-Based Backstepping Control of Tail-Sitter UAVs. *Actuators* **2021**, *10*, 119. https://doi.org/10.3390/act10060119

Academic Editor: William MacKunis, Muhammad Rehan

Received: 7 April 2021
Accepted: 29 May 2021
Published: 3 June 2021

Publisher's Note: MDPI stays neutral with regard to jurisdictional claims in published maps and institutional affiliations.

Copyright: © 2021 by the authors. Licensee MDPI, Basel, Switzerland. This article is an open access article distributed under the terms and conditions of the Creative Commons Attribution (CC BY) license (https://creativecommons.org/licenses/by/4.0/).

1. Introduction

Different variants of unmanned aerial vehicles (UAVs) have received attention in recent times due to potentially diverse types of applications, including surveillance, exploration, and transportation, to name a few. Hybrid vertical takeoff and landing (VTOL) air vehicles with qualities of both rotary-wing and fixed-wing aircraft can hover like rotary-wing aircraft or fly with high speed like fixed-wing aircraft. Consequently, hybrid VTOL UAVs can achieve a few missions that are regularly unthinkable for either fixed-wing or rotary-wing elevated robots alone [1]. There are different types of VTOL aircraft such as tail-rotor, tail-sitter, tilt-wing, and extra-propulsion [2]. The tail-sitter is the simplest one because it does not require supplementary actuators to perform the VTOL maneuver. Many researchers have explored small-sized tail-sitters. For instance, Bapst et al. [3] proposed a twin-rotor tail-sitter VTOL aircraft containing a flying wing with two rotors and elevons and a single controller for all flight modes and validated their work through outdoor experiments. Forshaw et al. [4] presented a concept of twin helicopter rotor tail-sitters. In [5], the researchers proposed a full-altitude controller for hovering, transition, and level flight. Oosedo et al. [6] designed a quadrotor tail-sitter UAV with high accuracy in altitude control in both hovering and level-flight modes. Later, Oosedo et al. have provided strategies for optimal transition from hovering to level flight [7] through normal transition, minimizing the transition time, and minimizing the transition time with constant altitude. Wang et al. [8] designed and implemented a low-cost quadrotor tail-sitter UAV with half

the power consumed in a typical quadrotor, as per flight test results with all VTOL maneuvers. In [9], a VertiKUL quadrotor tail-sitter UAV with no controlling surface, but operating in all three modes, was designed.

Figure 1 illustrates a quadrotor tail-sitter UAV with four tilted rotors to provide the lift force in vertical flight mode and the thrust during level flight. A hybrid quadrotor tail-sitter VTOL UAV can switch between hovering mode to level-flight mode and vice versa by rotating the aircraft's pitch angle about almost 90° as shown in Figure 2.

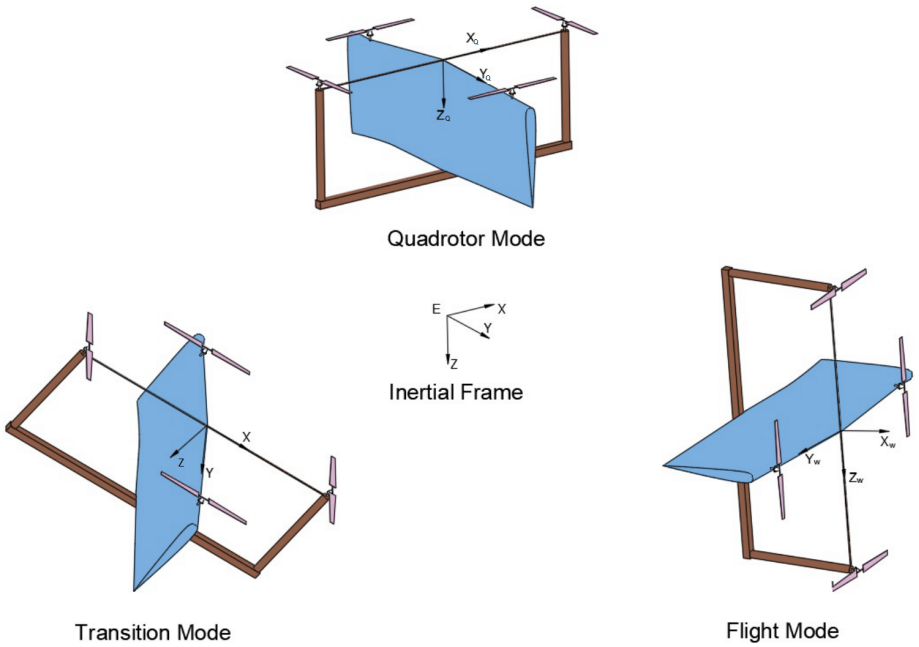

Figure 1. Quadrotor tail-sitter UAV.

Mathe et al. [10] listed some generic low-cost platforms and application fields of air vehicles using vision and control methods while emphasizing the sensor suites used for railway inspection. Trotta et al. [11] proposed network architecture and supportive optimization frameworks allowing UAVs to execute city-scale video monitoring of points of interest validated via imitation of a city environment with live traffic updates from a real bus transportation network using a UAV scheduler and Mixed Integer Linear Programming (MILP) techniques. Otto et al. [12] provided a literature review of optimization methods to civil applications of UAVs by describing drone applications and outline features applicable to operations planning, and providing insights into emerging modeling methodologies. Other researchers demonstrated (i) the level of throughput provided to a set of areas and (ii) the amount of energy exchanged with the grid by the ground sites for UAV-aided cellular networks [13]. The J-MATE model designed for optimal energy and throughput through revenue and cost components for large-problem instances shows out-performance of earlier methods.

Several control strategies are present in the literature for trajectory-tracking. In [14], model prediction-based cascaded control is presented for trajectory-tracking of a VTOL tail-sitter UAV in the hovering mode, with simulation conducted in a HIL (hardware in the loop) environment. Lyu et al. [15] presented a hierarchical control method to achieve autonomous flight with vertical takeoff, hovering, transition, level flight, and landing of a quadrotor tail-sitter UAV. Flight tests with manual and fully autonomous flight modes show a minimal altitude drop between different flight modes. Li et al. [16] presented a robust nonlinear controller for flight mode transition between hovering to level-flight mode where tail-sitter aircraft model with uncertainties including nonlinear terms, external disturbances, and parametric uncertainties.

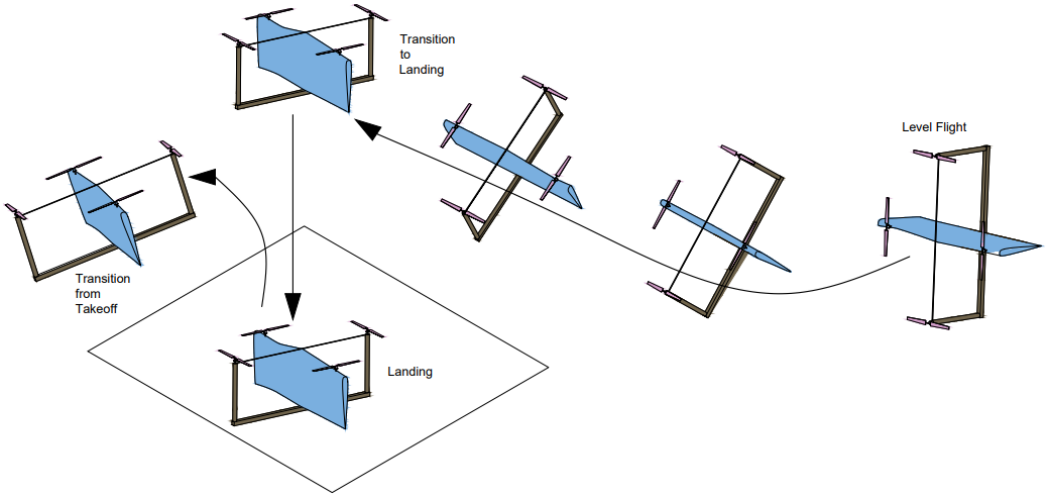

Figure 2. Takeoff and landing of tail-sitter quadrotor UAV.

Zhou et al. [17] proposed novel trajectory planning algorithms for a UAV under the constraints of system positioning accuracy while correcting the error during the flight process of a UAV. For the shortest path under the multiple constraints and minimum errors, a genetic algorithm (GA) helps to validate the results experimentally. Dynamic modeling, control law design, and hardware implementation are provided after deriving the dynamic model using the Newtonian method [18]. The control is designed for both modes—hovering and level-flight mode—to control the vehicle. The approach is implemented on a low-cost DSP-based Embedded Flight Control System (EFCS) for autonomous flight.

Zhou et al. [19] presented a combined control framework for a quadrotor tail-sitter UAV that deals with hovering and level-flight modes and allows continuous transition between these modes as per the directed velocity. The controller is also used to study the UAV's equilibrium state, mainly during a wind gust. Swarnkar et al. [20] presented the development of a 6-DOF flight dynamics model, with a comprehensive description of wing aerodynamics, prop wash modeling, and flight dynamics. Quaternions represent the aircraft's attitude to avoid singularity related to Euler angles, and a nonlinear controller uses a dynamic inversion method for the whole flight regime. Lyapunov-based control provides [21] trajectory-tracking for fixed-wing MAV. Simulation done in MAV3Dsim validates the efficacy of the control law. Brezoescu et al. [22] applied an adaptive backstepping scheme on fixed-wing UAV in the existence of unknown crosswind, and adaptive laws are proposed for disturbance estimation and validated through simulation results. Hajiloo et al. [23] presented nonlinear dynamics of single rotor spherical UAV and backstepping controller design based on it that works well for trajectory-tracking. Espinoza et al. [24] designed a controller based on backstepping and sliding modes implemented on fixed-wing UAV and studied which controller performance is more suitable for UAV. Sartori et al. designed a backstepping controller for fixed-wing UAVs on micro-controller and experimental data logged, endorsing the applicability controller [25]. Lungu et al. [26] presented a backstepping and dynamic inverse-based automatic landing system for fixed-wing UAV with wind gusts and atmospheric disturbances.

Rubi et al. review the relevant path following algorithms for quadrotors [27]. The simulation results with two control-oriented algorithms (Feedback Linearization and Backstepping) and two geometric algorithms (Nonlinear Guidance law (NLGL) and Carrot-Chasing) help to solve the path following problem. The backstepping method achieved the best performance in terms of path distance and yaw error and the best behavior out of the path and at high velocities. Lyu et al. [28] presented a control method with disturbance observer (DOB) to improve the hovering accuracy in crosswind flow. A nonlinear flight control method is designed for a fixed-wing UAV with an extended state observer (ESO) [29]. A multiple observer-based anti-disturbance control scheme uses disturbance observer-based (DO) and extended state observer (ESO)-based controller.

Experiments carried out for the payload oscillation disturbance and hybrid disturbances, robustness, and effectiveness are compared with the PID control method [30].

In this paper, we address two major issues for tail-sitter quadrotor UAVs: (i) Trajectory-tracking (ii) Compensate the effect of external disturbance on a tail-sitter UAV. For these, we present

- a robust controller for tail-sitter UAVs development using the backstepping technique;
- a nonlinear disturbance observer for both periodic and wind-gust-type disturbances.

A combination of nonlinear observer and backstopping control law ensures robustness for all three modes—Quadrotor mode, Transition mode, and level-flight mode—and ensures a robust approach for the whole flight envelope. Lyapunov stability analysis provides overall closed-loop stability and robustness. The controller's performance is demonstrated through trajectory-tracking simulations with applied disturbance in quadrotor, takeoff, and landing phases.

The rest of this paper is organized as follows: Problem formulation and quadrotor tail-sitter dynamics are presented in Section 2. In Section 3, we design a nonlinear observer to estimate the external disturbances. Next, a nonlinear observer-based backstepping controller is designed for hovering mode, takeoff, landing phase, and level-flight mode in Section 4. Simulation results are presented to demonstrate the efficacy of controller in Section 5 and concluding remarks are presented in Section 6.

2. Problem Formulation

Next, we describe tail-sitter UAV dynamics and control objectives. Figure 3 illustrates a quadrotor tail-sitter UAV with four tilted rotors to provide the lift force in vertical flight mode and the thrust during level flight. For control, the desired trajectory command is given to the quadrotor tail-sitter manually or by an upper-level motion planner. The tail-sitter UAV produces no significant lift and drag in a takeoff phase and landing phase. Therefore, we assume that the tail-sitter UAV acts as a quadrotor. The four input signals $[U_1\ U_2\ U_3\ U_4]$ control the vehicle's motion as done in the quadcopter. The tail-sitter UAV can switch between hovering mode to level-flight mode and vice versa by rotating the aircraft's pitch angle about almost 90° degree. In transition phase, control over x and y positions are disabled, and the objective is to maintain altitude and orientation. After completing transition, the vehicle enters the level-flight mode, and acts as a fixed-wing UAV. Please note that the role of yaw and roll is reversed in quadcopter and fixed-wing modes, respectively.

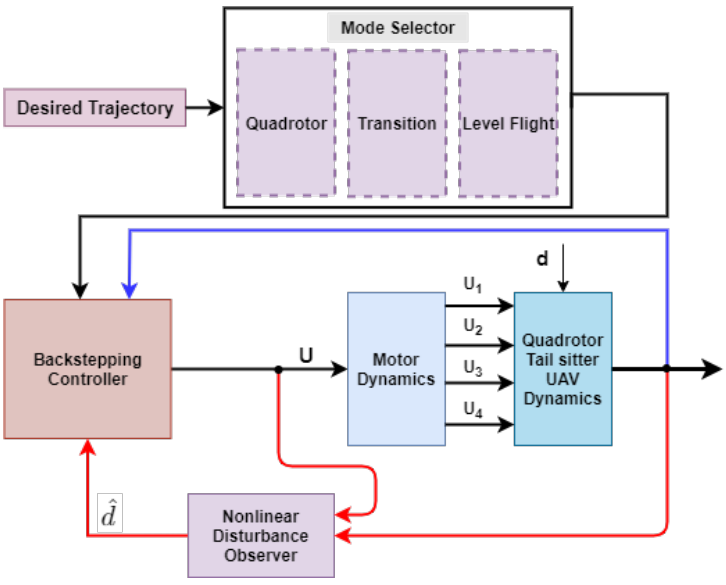

Figure 3. Controller Block Diagram.

A mathematical model of the quadrotor tail-sitter UAV is developed using the Newtonian or Lagrangian approach. As per [31], for u, v and w as the X, Y and Z directional body-axis velocities, and p, q and r as the angular velocities, the flight dynamics are

$$\dot{u} = rv - qw + g\cos\theta\cos\psi - \frac{L\cos\alpha + D\sin\alpha}{m} \quad (1)$$

$$\dot{v} = pw - ru + g\cos\theta\sin\psi \quad (2)$$

$$\dot{w} = qu - pv + g\sin\theta - \frac{L\sin\alpha + D\sin\alpha}{m} - \sum_{i=1}^{4}\frac{T_i}{m} \quad (3)$$

$$\dot{p} = \frac{qr(I_{yy} - I_{zz})}{I_{xx}} - \frac{I_r r}{I_{xx}}\sum_{i=1}^{4}(-1)^i\Omega_i + \frac{l(T_4 - T_2)}{I_{xx}} \quad (4)$$

$$\dot{q} = \frac{pr(I_{zz} - I_{xx})}{I_{yy}} + \frac{I_r q}{I_{yy}}\sum_{i=1}^{4}(-1)^i\Omega_i + \frac{l(T_1 - T_3)}{I_{yy}} \quad (5)$$

$$\dot{r} = \frac{pq(I_{xx} - I_{yy})}{I_{zz}} + \frac{1}{I_{zz}}\sum_{i=1}^{4}(-1)^i Q_i, \quad (6)$$

where I_{xx}, I_{yy} and I_{zz} are the fuselage moment of inertia around each axes, I_r is the propeller gyroscopic effect, m is the fuselage mass, g is the gravitational acceleration, l is the distance from the motor to the center of gravity, ϕ is the roll angle, θ is the pitch angle, and ψ is the yaw angle, Ω_i is the propeller revolution speed of i-th rotor, such that

$$V = \sqrt{V_x^2 + V_y^2 + V_z^2},\ \alpha = \arctan\left(\frac{V_z}{V_x}\right), T = C_T\rho\Omega^2 d^4$$

$$L = \frac{1}{2}\rho V^2 S C_l(\alpha),\ D = \frac{1}{2}\rho V^2 S C_d(\alpha),\ Q = C_Q\rho\Omega^2 d^5,$$

where S is the wing area, V is the velocity, ρ is the air density, d is rotor diameter, c is the drag coefficient, k is a constant, α is an Angle of Attack (AoA), L is the lift force, and D is the drag force. T and Q is trust and torque produced by propellers, d is the diameter of the propeller. C_l is a lift coefficient, C_d is a drag coefficient, C_T is the thrust coefficient and C_Q is the torque coefficient. For conventional tail-sitter quadrotor C_T, C_Q, ρ, d are constants, trust T and Q are proposal to propeller revolution speed so input of $[U_1\ U_2\ U_3\ U_4]$ can be expressed as

$$\begin{aligned} U_1 &= k(\Omega_1^2 + \Omega_2^2 + \Omega_3^2 + \Omega_4^2) \\ U_2 &= kl(\Omega_4^2 - \Omega_2^2) \\ U_3 &= kl(\Omega_1^2 - \Omega_3^2) \\ U_4 &= c(-\Omega_1^2 + \Omega_2^2 - \Omega_3^2 + \Omega_4^2) \\ \Omega &= (\Omega_2 + \Omega_4 - \Omega_1 - \Omega_3), \end{aligned}$$

where Ω is representing the overall residual propeller angular speed, k is thrust constant, c is torque constant and l is length of arm.

Although there are no significant aerodynamic forces and moments created during the vertical takeoff phase, hovering mode, and landing phase, the total forces and moments are only due to thrust. Therefore, the quadrotor tail-sitter UAV is considered a quadrotor for analysis purposes. The dynamical equations for quadrotor mode in the hybrid frame as given in [32] are

$$\ddot{\phi} = \left(\frac{I_{yy} - I_{zz}}{I_{xx}}\right)\dot{\theta}\dot{\psi} - \frac{I_r}{I_{xx}}\dot{\psi}\Omega + \frac{U_2}{I_{xx}} + d_\phi \tag{7}$$

$$\ddot{\theta} = \left(\frac{I_{zz} - I_{xx}}{I_{yy}}\right)\dot{\phi}\dot{\psi} + \frac{I_r}{I_{yy}}\dot{\theta}\Omega + \frac{U_3}{I_{yy}} + d_\theta \tag{8}$$

$$\ddot{\psi} = \left(\frac{I_{xx} - I_{yy}}{I_{yy}}\right)\dot{\phi}\dot{\theta} + \frac{U_4}{I_{zz}} + d_\psi \tag{9}$$

$$\ddot{x} = (\cos\phi \sin\theta \cos\psi + \sin\phi \sin\psi)\frac{U_1}{m} + d_x \tag{10}$$

$$\ddot{y} = (\cos\phi \sin\theta \sin\psi - \sin\phi \cos\psi)\frac{U_1}{m} + d_y \tag{11}$$

$$\ddot{z} = -g + \cos\phi \cos\theta \frac{U_1}{m} + d_z. \tag{12}$$

State vector can be defined for position (10)–(12) and attitude subsystem (7)–(9) as, $X = [P\ \dot{P}\ O\ \dot{O}]^T \in \mathcal{R}^{12}$, where $P = [x\ y\ z]^T$, $O = [\phi\ \theta\ \psi]^T$, and $d_p = \begin{bmatrix} d_x\ d_y\ d_z \end{bmatrix}$, $d_o = \begin{bmatrix} d_\phi\ d_\theta\ d_\psi \end{bmatrix}$ are the external disturbances.

The control objectives of this study are

- Design a nonlinear disturbance observer for model uncertainty as well as wind gust (external) disturbances while in takeoff phase, hovering mode and landing phase.
- To design control laws using backstepping technique for quadrotor tail-sitter UAVs to track the given trajectory.

3. Nonlinear Observer Design

The external disturbance, such as wind field, has a significant effect on tail-sitter quadrotor UAVs' stability, particularly in the takeoff and landing phase. In this section, we develop a nonlinear observer to estimate the uncertainties using an observer proposed in [33,34]. The following assumption is assumed for the disturbances d used during backstepping controller design and stability analysis.

Assumption 1. *The disturbance and derivative of disturbance are bounded:*

$$||\dot{d}_p(t)|| \leq D_p, \quad ||\dot{d}_o(t)|| \leq D_o \quad t > 0,$$

where D_p and D_o are positive constants.

Similarly, a nonlinear disturbance observer proposed by Yang et al. [35] and Viswanath et al. [36], can be implemented for both the position and attitude subsystems:

$$\dot{n}_p = -L_p n_p - L_p\left(L_p\dot{P} + G + \frac{1}{m}U_p\right), \quad \hat{d}_p = n_p + L_p\dot{P}, \tag{13}$$

$$\dot{n}_o = -L_o n_o - L_o\left(L_o\dot{O} + \Phi(O,\dot{O}) - U_o\right), \quad \hat{d}_o = n_o + L_o\dot{O}, \tag{14}$$

where $U_p = R(O)E_3U_1$, $U_o = \Psi(O)[U_2\ U_3\ U_4]^T$ ($U_i, i = 1,\ldots,4$) are shown in Figure 3, and $\hat{d}_j, j = p, o$ is the disturbance estimation, n_j is the observer state vector, $\zeta_j = L_j I_{3\times 3}$, $\zeta_j > 0$ are the tunable gain matrices, $G = [0\ 0\ -g]^T$, m = mass, $R(O)$ = rotation matrix and E_3 is unit vector basis associated with the earth fixed frame (I). $\Psi(O) = [IE_M(O)]^{-1}$ where $E_M(O)$ = Euler matrix.

Lemma 1 ([37]). *For a smooth system $\dot{x} = f(x)$, $x \in R^n$, with $f(0) = 0$ and a Lyapunov candidate function $V(V(0) = 0)$, let $x(0) \in \mathbf{C} \subset R^n$. Along any trajectory $x : R^+ \to R^n$, starting in $\mathbf{C}$, the following differential disparity is satisfied with $\beta > 0$*

$$\frac{d}{dt}\{V(x(t))\} < -\alpha V(x(t)) + \beta, \quad \forall t \geq 0 \text{ with } x(0) \in \mathbf{C}, \tag{15}$$

where α as a tunable positive parameter.

Proposition 1 ([37]). *Under Assumption 1, for an adequately large T^* there exist appropriate observer gains $L_j > 0, j = p, o$, for prescribed asymptotic estimation of observers (13) and (14) for every $\epsilon > 0$ there exist L_j^* for all $L_j \geq L_j^*$, the observer errors satisfy*

$$||e_{d_j}(t)||^2 \leq \epsilon, \ \ \forall t \geq T^*, \ \ j = p, o. \tag{16}$$

Proof. We rewrite (7)–(12) as

$$\ddot{P} = G + \frac{U_p}{m} + d_p, \ \ \ddot{O} = \Phi(O, \dot{O}) + U_o. \tag{17}$$

By differentiating (13) and using (17), we obtain

$$\begin{aligned} \dot{\hat{d}}_p &= \dot{n}_p + L_p \ddot{P} = -L_p n_p - L_p \left(L_p \dot{P} + G + \frac{U_p}{m} \right) + L_p \left(G + \frac{U_p}{m} + d_p \right) \\ &= -L_p \left(n_p + L_p \dot{P} \right) + L_p d_p = -L_p e_{d_p}. \end{aligned} \tag{18}$$

Similarly, we can show that

$$\dot{\hat{d}}_o = -L_o e_{d_o}, \tag{19}$$

for error terms $e_{d_j} = \hat{d}_j - d_j, j = p, o$, and using (18) and (19), the error derivatives are expressed as

$$\dot{e}_{d_j} = -\dot{d}_j - L_j e_{d_j}. \tag{20}$$

For a positive definite function defined in terms of error term e_{d_j}, given by

$$V_{1j} = e_{d_j}^T e_{d_j}, \tag{21}$$

and using Assumption 1, (20) and the inequality $-2e_{d_j}^T \dot{d}_j \leq ||e_{d_j}||^2 + ||\dot{d}_j||^2$, the time derivative of V_{1j} can be expressed as

$$\begin{aligned} \dot{V}_{1j} = 2e_{d_j}^T \dot{e}_{d_j} = -2e_{d_j}^T L_j e_{d_j} - 2e_{d_j}^T \dot{d}_j &\leq -2e_{d_j}^T L_j e_{d_j} + ||e_{d_j}||^2 + ||\dot{d}_j||^2 \\ &\leq (-2L_j + 1) V_{1j} + D_j^2. \end{aligned} \tag{22}$$

It turns out that the inequality (22) takes the form of (15) with $\alpha = -2L_j + 1$ and $\beta = D_j^2$, i.e., for $j = p, o$ such types of α, β exist. A lower bound on the observer gains L_j indicated by L_j^*, i.e., $L_j^* \leq L_j$ ensures that $(-2L_j + 1) \leq (-2L_j^* + 1)$, and so $\dot{V}_{1j}(t) \leq (-2L_j^* + 1) V_{1j}(t) + D_j^2$.

Therefore, to ensure $V_{1j}(t) = ||e_{dj}||^2 \leq \epsilon, \ \ \forall t \geq T^*; \ \ j = p, o$, we can choose L_j^* such that $(-2L_j^* + 1)\epsilon + D_j^2 = 0$, that is

$$L_j^* = \frac{1}{2} \left(\frac{D_j^2}{\epsilon} + 1 \right). \tag{23}$$

□

4. Backstepping Control Design

This section develops a robust controller using a backstepping technique [38–40] for the takeoff phase, hovering, transition, level-flight modes, and landing phase. The quadrotor tail-sitter UAV is an underactuated system used in most vehicles that need to control altitude and position using only four inputs [7].

4.1. Quadrotor Mode

We formulate nonlinear observer-based control law for the quadrotor mode using the backstepping method. Using Equations (10)–(12) let us consider position subsystem as

$$\dot{P}_{Q1} = P_{Q2}, \ \dot{P}_{Q2} = -g + \frac{1}{m}U_p + d_p. \tag{24}$$

For position tracking, the error is defined as $e_1 = P_{Q1_d} - P_{Q1}$. The time derivative is given as

$$\dot{e}_1 = \dot{P}_{Q1_d} - \dot{P}_{Q1} = \dot{P}_{Q1_d} - P_{Q2}. \tag{25}$$

Lyapunov function candidate for position subsystem is chosen as

$$V_{QP_1} = \frac{1}{2}e_1^T e_1. \tag{26}$$

Now, with velocity tracking error defined as $e_2 = P_{Q2_d} - P_{Q2}$, and using (25), we get

$$\dot{e}_1 = \dot{P}_{Q1_d} - P_{Q2_d} + e_2, \tag{27}$$

where P_{Q2_d} is virtual input designed to stabilized $\dot{e}_1$, such that

$$P_{Q2_d} = \dot{P}_{Q1_d} + c_1 e_1, \ \dot{P}_{Q2_d} = \ddot{P}_{Q1_d} + c_1 \dot{e}_1, \tag{28}$$

where c_1 is positive definite matrix, and by substituting (28) into (27), we obtain

$$\dot{e}_1 = e_2 - c_1 e_1. \tag{29}$$

Lyapunov function candidate is chosen as

$$V_{QP_2} = \frac{1}{2}e_1^T e_1 + \frac{1}{2}e_2^T e_2. \tag{30}$$

Taking time derivative of (30) and using (28), we obtain

$$\dot{V}_{QP_2} = e_1^T \dot{e}_1 + e_2^T \dot{e}_2 = e_1^T(-c_1 e_1 + e_2) + e_2^T(\ddot{P}_{Q1_d} + c_1 \dot{e}_1 - \dot{P}_{Q2}). \tag{31}$$

Substituting (24) into (31), we obtain

$$\begin{aligned} \dot{V}_{QP_2} &= -e_1^T c_1 e_1 + e_1^T e_2 + e_2^T \left(\ddot{P}_{Q1_d} + c_1 \dot{e}_1 - \left(-g + \frac{1}{m}U_p + d_p \right) \right) \\ &= -e_1^T c_1 e_1 + e_2^T \left(e_1 + \ddot{P}_{Q1_d} + c_1 \dot{e}_1 + g - \frac{1}{m}U_p - d_p \right). \end{aligned} \tag{32}$$

Now, the Control law for the position sub system can be defined as

$$U_p = m\left(e_1 + c_1 \dot{e}_1 + g + \ddot{P}_{Q1_d} + c_2 e_2 - \hat{d}_p \right), \tag{33}$$

where c_2 is a positive definite matrix, Using (12), three components of U_P: $[U_1,\ U_x,\ U_y]$ are given as

$$U_1 = \frac{U_p}{\cos\phi\cos\theta}, \tag{34}$$

$$U_x = \frac{\cos\phi\sin\theta\cos\psi + \sin\phi\sin\psi}{\cos\phi\cos\theta}U_1, \tag{35}$$

$$U_y = \frac{\cos\phi\sin\theta\sin\psi - \sin\phi\cos\psi}{\cos\phi\cos\theta}U_1. \tag{36}$$

To compensate for the disturbance d_p to achieve improved robustness, we employ the nonlinear disturbance observer (13).

Theorem 1 ([37]). *For the error subsystem (25) with the disturbance observers (13) and (14), and the control signals (33) and (34), there exist positive definite matrices c_1, c_2 and L_p, resulting in*

$$0 < ||e_1||^2 + ||e_2||^2 \leq \epsilon,\ \forall\ t \geq T^* \tag{37}$$

for tracking errors e_1, e_2, and a chosen adequately large ϵ.

Proof. Lyapunov Function candidate can be defined as,

$$V_{QP} = V_{QP_1} + V_{QP_2}. \tag{38}$$

Considering (31), (33), from (38), we obtain

$$\begin{aligned}
\dot{V}_{QP} = \dot{V}_{QP_1} + \dot{V}_{QP_2} &= -e_1^T c_1 e_1 + e_1^T e_2 + e_2^T(\ddot{P}_{Q1_d} + c_1\dot{e}_1 - g + \frac{1}{m}U_p + d_p) \\
&- e_{dp}^T(L_p - \frac{1}{2}I_{3\times3})e_{dp} + \frac{1}{2}D_p^2 \\
&= -e_1^T c_1 e_1 - e_2^T c_2 e_2 + e_2^T(\hat{d}_p - d_p) - e_{dp}^T(L_p - \frac{1}{2}I_{3\times3})e_{dp} + \frac{1}{2}D_p^2 \\
&\leq -e_1^T c_1 e_1 - e_2^T c_2 e_2 - \frac{1}{2}e_2^T e_2 - e_{dp}^T L_p e_{dp} + \frac{1}{2}D_p^2 \\
&< \delta_1 V_{QP} + D_p^2,
\end{aligned} \tag{39}$$

where $\delta_1 = \min\{2\lambda_{min}(c_1), 2(\lambda_{\min}(c_2) - \frac{1}{2}), 2(\lambda_{min}(L_p - 1))\}$. □

The above gains are chosen to deliver any scale of the tunable $\lambda > 0$ so that (37) follows from Lemma 1. Yaw angle can be directly measured by the sensor and desired roll angle (ϕ_d) and pitch angle (θ_d) can be calculated using position and attitude subsystem. Reference trajectory for the attitude subsystem can be defined as $O_d = [\phi_d,\ \theta_d,\ \psi_d]^T$. The desired angles ϕ_d and θ_d can be obtained using (35) and (36) such that

$$U_x C_{\phi_d} C_{\theta_d} C_{\psi_d} = (C_{\phi_d} S_{\theta_d} C_{\psi_d}^2 + S_{\phi_d} S_{\psi_d} C_{\psi_d})U_1, \tag{40}$$

$$U_y C_{\phi_d} C_{\theta_d} S_{\psi_d} = (C_{\phi_d} S_{\theta_d} S_{\psi_d}^2 - S_{\phi_d} S_{\psi_d} C_{\psi_d})U_1. \tag{41}$$

Adding Equations (40) and (41) and dividing by C_{ϕ_d} and C_{θ_d}, we obtain

$$U_x C_{\psi_d} + U_y S_{\psi_d} = (\tan\theta_d)U_1, \tag{42}$$

ϕ_d and θ_d obtained from Equations (40)–(42):

$$\theta_d = \tan^{-1}\left(\frac{U_x C_{\psi_d} + U_y S_{\psi_d}}{U_1}\right), \tag{43}$$

$$\phi_d = \tan^{-1}\left(\frac{C_{\theta_d}(U_x S_{\psi_d} - U_y C_{\psi_d})}{U_1}\right), \tag{44}$$

$C_a = \cos a$, $S_a = \sin a$.

Using the same method, we define control law for the attitude subsystem

$$\dot{O}_{Q1} = O_{Q2}, \;\; \dot{O}_{Q2} = \Phi(O, \dot{O}) + U_o + d_o. \tag{45}$$

Defining the error in angle as $e_3 = O_{Q1_d} - O_{Q1}$, the time derivative is

$$\dot{e}_3 = \dot{O}_{Q1_d} - O_{Q2}. \tag{46}$$

Lyapunov candidate function can be

$$V_{QO_1} = \frac{1}{2} e_3^T e_3. \tag{47}$$

For error in angular velocity $e_4 = O_{Q2_d} - O_{Q2}$, the time derivative is

$$\dot{e}_4 = \dot{O}_{Q2_d} - \dot{O}_{Q2}, \tag{48}$$

and an appropriate Lyapunov function candidate can be

$$V_{QO_2} = V_{QO_1} + \frac{1}{2} e_4^T e_4, \tag{49}$$

and using (45), (46), the time derivative of (49) is given as

$$\dot{V}_{QO_2} \;\; = \;\; -e_3^T c_3 e_3 + e_3^T e_4 + e_4^T \left(\ddot{O}_{Q1_d} + c_3 \dot{e}_3 - \left(\Phi(O, \dot{O}) + U_o + d_o\right)\right). \tag{50}$$

The control law for the attitude subsystem can be defined as

$$U_o = e_3 + c_3 \dot{e}_3 - \Phi(O, \dot{O}) + \ddot{O}_{Q1_d} - \hat{d}_o + c_4 e_4. \tag{51}$$

Next, we prove the attitude counterpart of Theorem 1.

Theorem 2 ([37]). *Consider the attitude error subsystem (46) and (48) in closed loop with the disturbance observer designed as in (13), (14) and the control law designed according to (51). There exist positive definite gain matrices c_3, c_4 and L_o, such that the closed-loop attitude error satisfies*

$$\dot{V}_{QO} = \dot{V}_{QO_1} + \dot{V}_{QO_2} < \delta_2 V_{Q2} + D_o^2, \tag{52}$$

Proof. Lyapunov Function candidate can be defined as

$$V_{QO} = V_{QO_1} + V_{QO_2} \tag{53}$$

Considering (50), (51) and (53), we obtain

$$\begin{aligned}
\dot{V}_{QO} = \dot{V}_{QO_1} + \dot{V}_{QO_2} &= -e_3^T c_3 e_3 + e_3^T e_4 + e_4^T \left(\ddot{O}_{Q1_d} + c_3 \dot{e}_3 - \left(\Phi(O, \dot{O}) + U_o + d_o\right)\right) \\
&\quad - e_{do}^T (L_o - \frac{1}{2} I_{3\times 3}) e_{do} + \frac{1}{2} D_o^2 \\
&= -e_3^T c_3 e_3 - e_4^T c_4 e_4 + e_4^T (\hat{d}_o - d_o) - e_{do}^T (L_o - \frac{1}{2} I_{3\times 3}) e_{do} + \frac{1}{2} D_o^2 \\
&\leq -e_3^T c_3 e_3 - e_4^T c_4 e_4 - \frac{1}{2} e_4^T e_4 - e_{do}^T L_o e_{do} + \frac{1}{2} D_o^2 \\
&< \delta_2 V_{QO} + D_o^2,
\end{aligned} \tag{54}$$

where $\delta_2 = \min\{2\lambda_{min}(c_3), 2(\lambda_{\min}(c_4) - \frac{1}{2}), 2(\lambda_{min}(L_0 - 1))\}$. □

4.2. Transition Mode

The transition controller's main role is to allow the tail-sitter UAVs to change the flight mode from hovering to level flight and vice versa. During the maneuver, aerodynamic forces and propulsive forces are the two sources of force. Level flight is achievable in the rotary-wing configuration, where the thrust generated by the rotors is equal to the weight of the UAV. Quadrotor mode controller controls the initial phase, and the control law for the pitch angle is changed to directly control directed altitude and pitch angle without $x - y$ position control. When aerodynamic forces are substantial, the flight mode controller takes over. Transfer from quadrotor to level-flight mode happens when the wing reaches α_{stall}, i.e., $\theta_{Qsw} = \alpha_{stall} - \gamma_{des} - 90^\circ$.

We have divided the control action into three different sections appropriate for the three modes: quadrotor, transition, and level-flight mode. With the pitch angle less than a specific angle, say λ_1, the controller in action is the one in the quadrotor mode, and when the pitch angle exceeds another angle λ_2, the control action in play is the level-flight controller designed in the next subsection. When the pitch angle is between λ_1 and λ_2, the transition controller is active.

For the transition mode, as explained in [32], Equations (1)–(6) can be written in state space as

$$\begin{pmatrix} \dot{\phi} \\ \ddot{\phi} \\ \dot{\theta} \\ \ddot{\theta} \\ \dot{\psi} \\ \ddot{\psi} \\ \dot{z} \\ \ddot{z} \\ \dot{x} \\ \ddot{x} \\ \dot{y} \\ \ddot{y} \end{pmatrix} = \begin{pmatrix} x_2 \\ x_4 x_6 a_1 - a_2 x_6 \Omega + U_2 b_1 \\ x_4 \\ x_2 x_6 a_3 + a_4 x_4 \Omega + U_3 b_2 \\ x_6 \\ x_2 x_4 a_5 + U_4 b_3 \\ x_8 \\ x_4 x_{10} - x_2 x_{12} + g \sin x_3 - r_1 - U_1/m \\ x_{10} \\ x_6 x_{12} - x_4 x_8 - g \cos x_3 \cos x_5 - r_2 \\ x_{12} \\ x_2 x_8 - x_6 x_{10} + g \cos x_3 \sin x_5 \end{pmatrix}, \tag{55}$$

where $\dot{x}_1 = \dot{\phi} = p$, $\dot{x}_2 = \ddot{\phi} = \dot{p}$, $\dot{x}_3 = \dot{\theta} = q$, $\dot{x}_4 = \ddot{\theta} = \dot{q}$, $\dot{x}_5 = \dot{\psi} = \mathrm{r}$, $\dot{x}_6 = \ddot{\psi} = \dot{r}$, $\dot{x}_7 = \dot{z} = w$, $\dot{x}_8 = \ddot{z} = \dot{w}$, $\dot{x}_9 = \dot{x} = u$, $\dot{x}_{10} = \ddot{x} = \dot{u}$, $\dot{x}_{11} = \dot{y} = v$ and $\dot{x}_{12} = \ddot{y} = \dot{v}$, and $a_1 = \frac{I_{yy} - I_{zz}}{I_{xx}}$, $a_2 = \frac{I_r}{I_{xx}}$, $a_3 = \frac{I_{zz} - I_{xx}}{I_{yy}}$, $a_4 = \frac{I_r}{I_{yy}}$, and $a_5 = \frac{I_{xx} - I_{yy}}{I_{zz}}$, $b_1 = \frac{1}{I_{xx}}$, $b_2 = \frac{1}{I_{yy}}$, $b_3 = \frac{1}{I_{zz}}$, $r_1 = \left(\frac{L\cos\alpha + D\sin\alpha}{m}\right)$ and $r_2 = \left(\frac{L\sin\alpha + D\cos\alpha}{m}\right)$.

The control law for transition mode is obtainable by dividing the tail-sitter dynamics into four subsystems: roll, pitch, yaw, and altitude subsystems. First, we apply the backstepping control technique to the roll angle subsystem (roll angle and rate of change). The associated dynamics are

$$\begin{aligned} \dot{x}_1 &= x_2, \\ \dot{x}_2 &= x_4 x_6 a_1 - a_2 x_6 \Omega + U_2 b_1. \end{aligned}$$

For $e_1 = x_1 - x_{1d}$ (error between actual and desired roll angle), a positive definite function is defined: $V_{TM_1} = \frac{1}{2} e_1^2$, and time derivative is $\dot{V}_{TM_1} = e_1 \dot{e}_1 = e_1(x_2 - \dot{x}_{1d}) \leq -k_1 e_1^2$, $k_1 > 0$. To satisfy this condition, a virtual control $x_{2d} = \dot{x}_{1d} - c_1 e_1$ is chosen such that $e_2 = x_2 - x_{2d} = x_2 - \dot{x}_{1d} + k_1 e_1$. Time derivative of e_2 is $\dot{e}_2 = \dot{x}_2 - \ddot{x}_{1d} + c_1 \dot{e}_1$. Using these equations, we obtain

$$\dot{V}_{TM_1} = e_1(x_2 - \dot{x}_{1d}) = e_1 e_2 - k_1 e_1^2. \tag{56}$$

The next step is to enhance V_{TM_1} with a quadratic term in e_2 to obtain a positive definite $V_{TM_2} = V_{TM_1} + \frac{1}{2}e_2^2$. With a choice of control law U_2 given as

$$U_2 = \frac{1}{b_1}(-x_4x_6a_1 + a_2x_6\Omega + \ddot{x_1} - e_1 - k_1\dot{e_1} - e_2k_2), \tag{57}$$

the time derivative of V_{TM_2} is $\dot{V}_{TM_2} \leq -k_1e_1^2 - k_2e_2^2$ which guarantees asymptotic stable system for appropriately chosen $k_1, k_2 > 0$.

Using the same procedure, control law for the altitude, pitch and roll subsystems can be defined as

$$\begin{aligned}
U_1 &= m(-x_2x_{12} + x_4x_{10} + g\sin x_3 - r_1 - \ddot{x}_{7d} + e_7 - k_7\dot{e}_7 + k_8e_8), \;\; k_7, k_8 > 0,\\
U_3 &= \frac{1}{b_2}(-x_2x_6a_3 - a_4x_4\Omega + \ddot{x}_{3d} + k_3\dot{e}_3 - e_3 - k_4e_4), \;\; k_3, k_4 > 0,\\
U_4 &= \frac{1}{b_3}(-x_2x_4a_5 + \ddot{x}_{5d} - k_6e_6 - e_5 + k_5\dot{e}_5), \;\; k_5, k_6 > 0.
\end{aligned}$$

The quadrotor and transition modes' basic difference considers the lift and drag forces in the transition mode. So, if $\lambda_1 > \theta$, the control law U_1, U_2, U_3 and U_4 remains same as in the quadrotor mode. We have control over x and y axis so U_x and U_y control laws are defined as given in (33). If $\lambda_2 < \theta$, then the controller is switched into the level-flight controller, as described next.

4.3. Level-Flight Mode

Level-flight mode is a fixed-wing mode or airplane mode easily visualized using the right-hand fixed-wing axis system. Variables defined in dynamic Equations (1)–(6) of quadrotor tail-sitter UAV concern the quadrotor axis. It can be transformed from quadrotor axis to fixed-wing axis as shown in Figure 1, and defined as

$$\begin{bmatrix} V_x \\ V_y \\ V_z \end{bmatrix}_W = \begin{bmatrix} -V_z \\ V_y \\ V_x \end{bmatrix}_Q = R_Q^W \begin{bmatrix} V_x \\ V_y \\ V_z \end{bmatrix}_Q, \quad R_Q^W = \begin{bmatrix} 0 & 0 & -1 \\ 0 & 1 & 0 \\ 1 & 0 & 0 \end{bmatrix}. \tag{58}$$

To design a controller for level-flight mode, the complete mathematical model of the level-flight mode Equations (1)–(6) is changed as explained in (58). The control law for the yaw subsystem can be defined as shown in transition mode. Yaw angle subsystem, a positive definite function is defined: $V_{LC_1} = \frac{1}{2}e_1^2$ and time derivative of V_{LC_1} is

$$\dot{V}_{LC_1} = e_1\dot{e}_1 = e_1(x_2 - \dot{x}_{1d}) \leq -s_1e_1^2, \quad s_1 > 0. \tag{59}$$

A virtual control $x_{2d} = \dot{x}_{1d} - c_1e_1$ is chosen such that $e_2 = x_2 - \dot{x}_{1d} + s_1e_1$ and time derivative of e_2 is, $\dot{e}_2 = \dot{x}_2 - \ddot{x}_{1d} + c_1\dot{e}_1$, and $\dot{V}_{LC_1} = e_1e_2 - s_1e_1^2$. Now, V_{LC_1} with a quadratic term in e_2 to obtain a positive definite V_{LC_2} as explained in transition mode, and with a choice of control law U_4 given as

$$U_4 = \frac{1}{b_3}(x_4x_6a_1 - a_2x_6\Omega - \ddot{x}_{1d} + e_1 + s_1\dot{e}_1 + e_2s_2). \tag{60}$$

Therefore, $\dot{V}_{LC_2} \leq -s_1e_1^2 - s_2e_2^2$ guarantees asymptotic stable system for an appropriately chosen $s_1, s_2 > 0$.

Input for controlling the Pitch movement(U_3), Roll movement(U_2), and altitude (U_1) as well as x and y position (U_x and U_y) are calculated as

$$\begin{aligned}
U_1 &= m(-x_6x_{12} + x_4x_8 + g\sin x_3 + r_2 + \ddot{x}_{7d} + s_7\dot{e}_7 - e_7 - s_8e_8)\\
U_2 &= \frac{1}{b_1}(-x_4x_2a_5 + \ddot{x}_5 + s_5\dot{e}_5 - e_5 - s_6e_6)\\
U_3 &= \frac{1}{b_2}(-x_2x_6a_3 - a_4x_4\Omega + \ddot{x}_{3d} + s_3\dot{e}_3 - e_3 - e_4s_4)\\
U_x &= (-e_9 + \ddot{x}_9 + s_9\dot{e}_9 - s_{10}e_{10} - x_4x_{10} + x_2x_{12} + r_1)\\
U_y &= (-e_{11} + \ddot{x}_{11} + s_{11}\dot{e}_{11} - s_{12}e_{12} - x_2x_8 + x_6x_{10}).
\end{aligned}$$

Using these equations, the desired roll ϕ_d, pitch θ_d and yaw ψ_d angles are

$$\phi_d = \arctan\left(\frac{U_y}{U_x}\right),\ \ \theta_d = \arctan\left(\frac{U_y}{g\cos\phi_d}\right),\ \ \psi_d = \arctan\left(\frac{\Delta y}{\Delta x}\right). \tag{61}$$

We have shown development of suitable control signals for all three modes.

Theorem 3 ([37]). *Let the position error subsystem (25) in closed loop with the disturbance observer (13), (14) designed be controlled according to (33), (34) and attitude subsystem in closed loop with the disturbance observer (13) and (14). Under these conditions, designed according to (51), there exists an ensemble of gain matrices c_1, c_2, c_3, c_4, L_p and L_o such that the overall closed-loop control error vector $[e_1\ e_2\ e_3\ e_4]$ is bounded as follows*

$$||e||^2 \leq \epsilon\ \ \forall t \geq T^* \tag{62}$$

with any pre-selected precision $\epsilon > 0$ where T^* is sufficiently large.

Proof. Choosing a Lyapunov function candidate

$$V = V_{QP} + V_{QO} + \sum_{i=1}^{8} V_{TM_i} + \sum_{i=1}^{8} V_{LC_i}, \tag{63}$$

and differentiating (63), and using (52) and (54) we obtain

$$\begin{aligned}
\dot{V} &= \dot{V}_{QP} + \dot{V}_{QO} + \sum_{i=1}^{8}\dot{V}_{TM_i} + \sum_{i=1}^{8}\dot{V}_{LC_i}\\
&\leq -\delta_1 V_{QP_2} + \frac{1}{2}D_p^2 - \delta_2 V_{QO_2} + \frac{1}{2}D_o^2 - k_f e_f^2 - k_n e_n^2 - s_i e_i^2 - s_j e_j^2\\
&< -\delta V + \gamma - k_f e_f^2 - k_n e_n^2 - s_i e_i^2 - s_j e_j^2,
\end{aligned} \tag{64}$$

where $\delta = \min\{\delta_1, \delta_1\}$ and $\gamma = \frac{1}{2}D_p^2 + \frac{1}{2}D_o^2$, D_P and D_o are bounded as per the Assumption 1 and $k_f > 0$, $f = 1,3,5,7$, $k_n > 0$, $n = 2,4,6,8$. And $s_i > 0$, $i = 1,3,5,7,9,11$ and $s_j > 0$, $j = 2,4,6,8,10,12$. Since δ_1 and δ_2 are both tunable, it follows from Lemma 1 that for any desired $\epsilon > 0$, there exists an ensemble of gain matrices c_1, c_2, c_3, c_4, L_p and L_o such that the magnitude of both the position and attitude errors do not exceed ϵ on sufficiently long control horizons. The tracking control of tail-sitter UAVs is hence complete. □

5. Simulation Results

Next, we evaluate the backstepping controller's performance for trajectory-tracking, which contains vertical takeoff phase, hovering, transition, and level-flight modes, landing phase. Simulation parameters are shown in Table 1.

Table 1. Simulation Parameters.

Parameters	Value
g	$9.8\ \mathrm{m{\cdot}s^{-2}}$
Mass (m)	1.2 kg
length (l)	1 m
$I_{xx},\ I_{yy}$	$7.5 \times 10^{-3}\ \mathrm{kg{\cdot}m^2}$
I_{zz}	$1.3 \times 10^{-3}\ \mathrm{kg{\cdot}m^2}$
J_r	$7.5 \times 10^{-5}\ \mathrm{kg{\cdot}m^2}$
drag coefficient (d)	7.5×10^{-7}
lift coefficient (b)	7.5×10^{-3}

Initial conditions are $[x\ y\ z\ \phi\ \theta\ \psi] = [0.1\ 0.1\ 0\ 0\ 0\ 0.01]$. With quadrotor tail-sitter in hovering mode, external disturbance is applied, and parametric uncertainty and external parameter are added to each subsystem. Two types of external disturbances are applied (i) $[d_x\ d_y\ d_z] = [1+\sin 2t\ 1+\sin 2t\ 1+\sin 2t]$ and $[d_\phi\ d_\theta\ d_\psi] = [\sin 2t\ \sin 2t\ \sin 2t]$ (periodic disturbances) and (ii) Von Karman wind gust model. The nonlinear disturbance observer gains are designed as $L_p = [10\ 10\ 10]^T$ for the position subsystem and $L_o = [30\ 30\ 30]^T$ for attitude.

5.1. Trajectory-Tracking

The performance during different modes is evaluated and the results are shown. The timeline has been shown for clarity but is not drawn to scale. As shown in Figure 4, simulation for trajectory-tracking is carried out for 441 s which includes quadrotor mode, transition phase and level-flight mode.

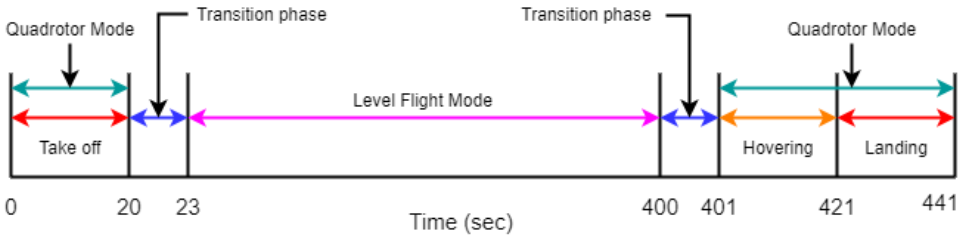

Figure 4. Timeline for trajectory-tracking.

Position tracking during quadrotor and transition phase is shown in Figure 5; it can be observed that during quadrotor mode (0 to 20 s) the desired trajectory for position subsystem is tracked effectively.

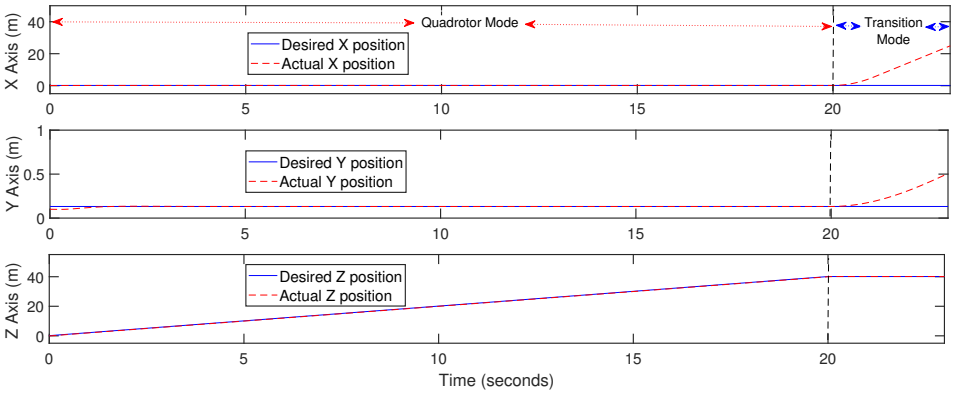

Figure 5. Position tracking during quadrotor mode and transition mode.

When in transition mode (20 to 23 s), we do not have control over the x and y position, which is why x and y position curves diverged but altitude is effectively controlled. Figure 6 shows the simulation outcome for UAV attitude control during quadrotor and transition modes. Yaw angle is measured, and roll and pitch angles are calculated. When in quadrotor mode, the desired yaw angle is effectively tracked. In transition mode, the UAV is commanded to rotate 80° about pitch angle and a constant roll and yaw angle. Figure 6 shows that the transition happens successfully without a change in roll and yaw angles.

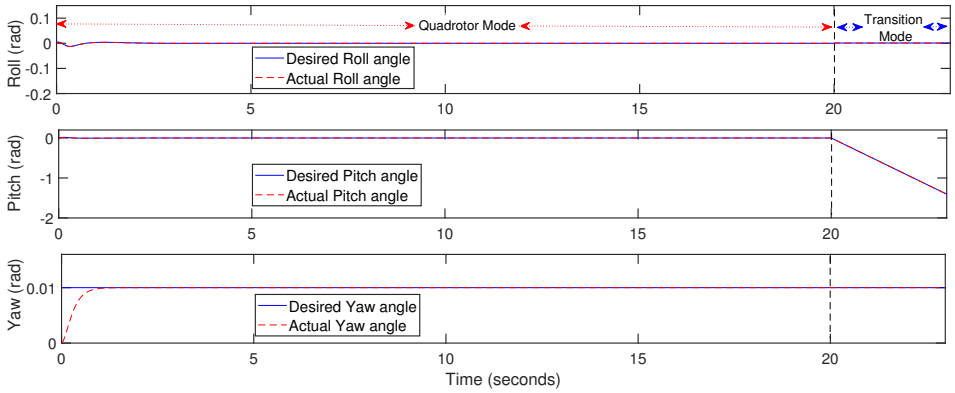

Figure 6. Attitude tracking during quadrotor mode and transition mode.

Figures 7 and 8 show the overall position and attitude control by the proposed backstepping controller.

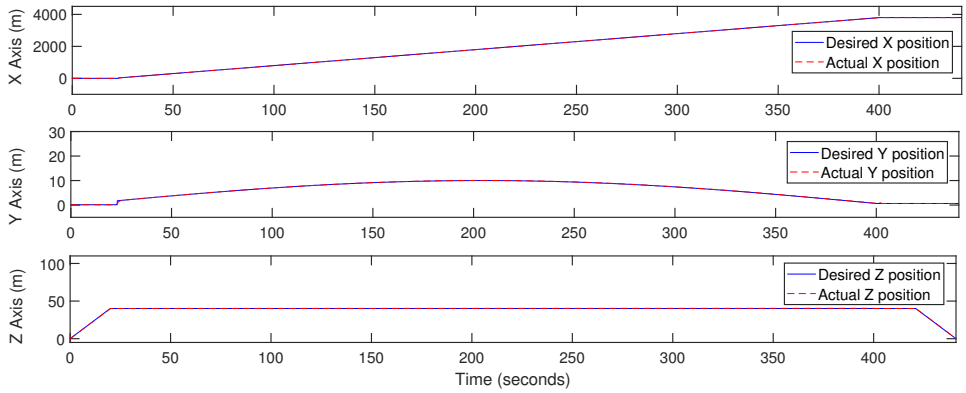

Figure 7. Position tracking by backstepping controller.

After the transition, the vehicle is converted to a conventional fixed-wing UAV. For $23 < t < 400$ s, the UAV is commanded to travel at 10 m/s velocity in level-flight mode. The trajectory is effectively controlled without altitude drop, and a 10 m/s velocity is maintained. In the period $400 < t < 401$ s, the UAV is commanded to rotate about its pitch angle from $-80°$ to $0°$, and transits from level-flight mode to quadrotor mode where there is no position change in x and y direction. For $401 < t < 421$ s, UAV commanded to hold altitude at 40 m and $421 < t < 441$ s it commanded to activate landing phase. As shown in Figures 7 and 8, The backstepping controller tracks the desired trajectory, and the simulation results validate the controller's performance.

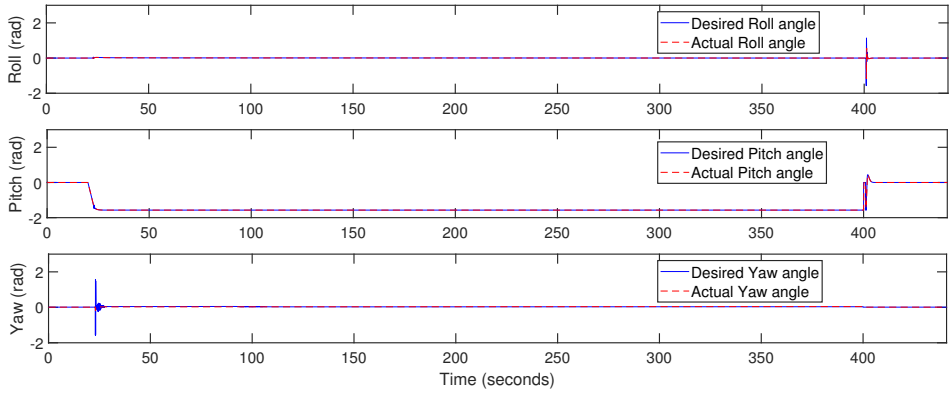

Figure 8. Attitude tracking by backstepping controller.

Figure 9 shows the three-dimensional trajectory-tracking, and Figure 10 shows the velocity profile during the same. It is observed that the proposed controller facilitates effective tracking of the desired trajectory.

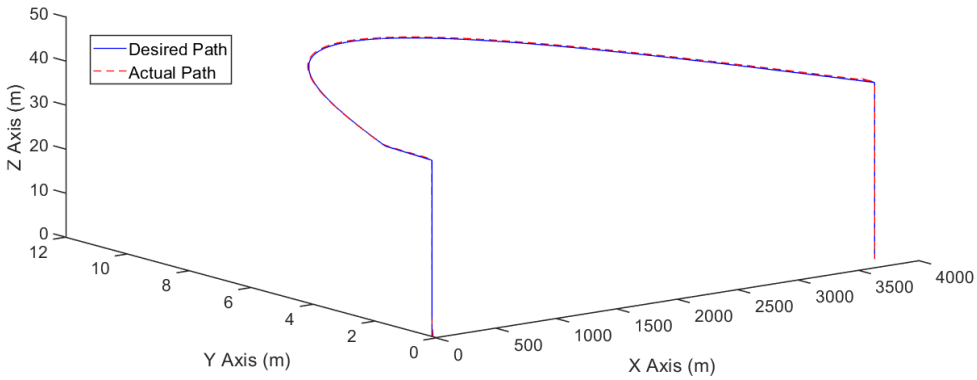

Figure 9. Trajectory-tracking.

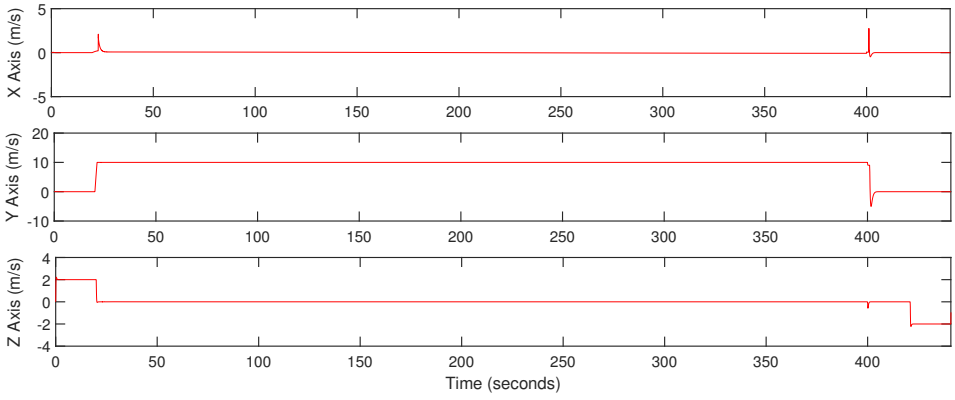

Figure 10. Velocity profile.

5.2. Quadrotor Mode with External Disturbance

This section simulates the takeoff phase, hovering mode, and the landing phase with external disturbance. As shown in Figure 4, for this simulation only quadrotor mode, $0 < t < 20$ (takeoff phase) and $401 < t < 441$ (hovering and landing phase) considered. For robustness against disturbance, we design a nonlinear disturbance observer. We evaluate the disturbance observer's performance and the disturbance impact on the position and attitude subsystem of UAV. Simulation is performed for 60 s, in which t = 0 to t = 20 s UAV commanded to takeoff with 2 m/s constant velocity, t = 20 to t = 40 s, tail-sitter is in hovering mode and t = 40 to t = 60 s it commanded to landing. During this

period, two types of external disturbance are applied to it. First, periodic disturbances $[d_x\ d_y\ d_z] = [1+\sin 2t\ 1+\sin 2t\ 1+\sin 2t]$ and $[d_\phi\ d_\theta\ d_\psi] = [\sin 2t\ \sin 2t\ \sin 2t]$ are applied.

Figure 11 shows the position tracking when a periodic disturbance is applied during flight. There is no significant change in position. Figure 12 shows the attitude tracking, there is no substantial change in the attitude subsystem of the UAV. These results validate the proposed backstepping controller performance.

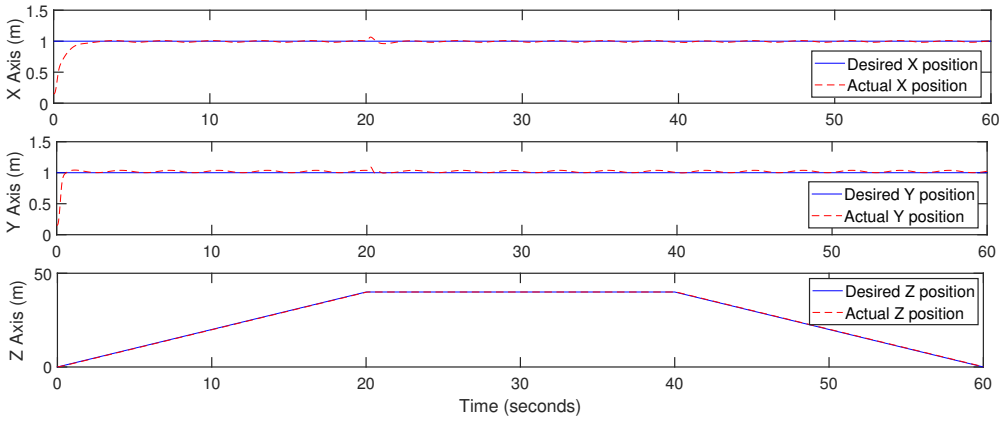

Figure 11. Position tracking when disturbance $[1+\sin(2t)\ 1+\sin(2t)\ 1+\sin(2t)]$ applied.

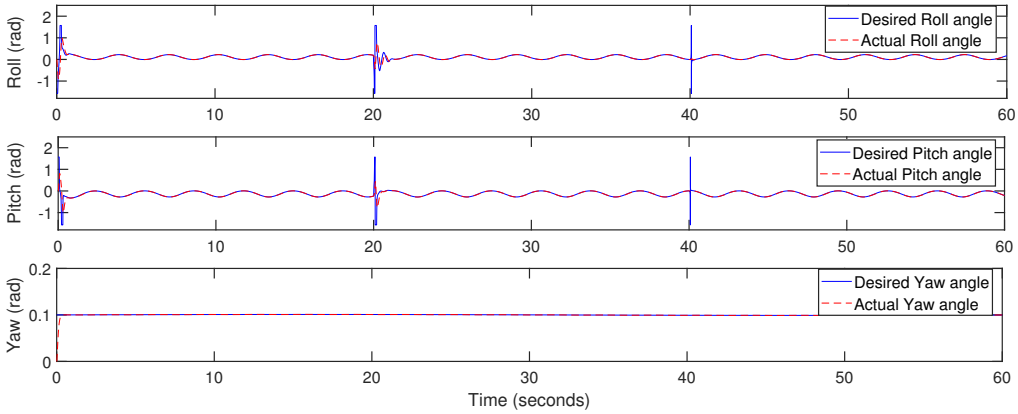

Figure 12. Attitude tracking when disturbance $[\sin(2t)\ \sin(2t)\ \sin(2t)]$ applied.

Figures 13 and 14 show the disturbance observer performance for the position and attitude subsystems, and the error in estimating these disturbances are shown in Figure 15 and Figure 16 respectively. We observe an error in millimeters in Figure 15.

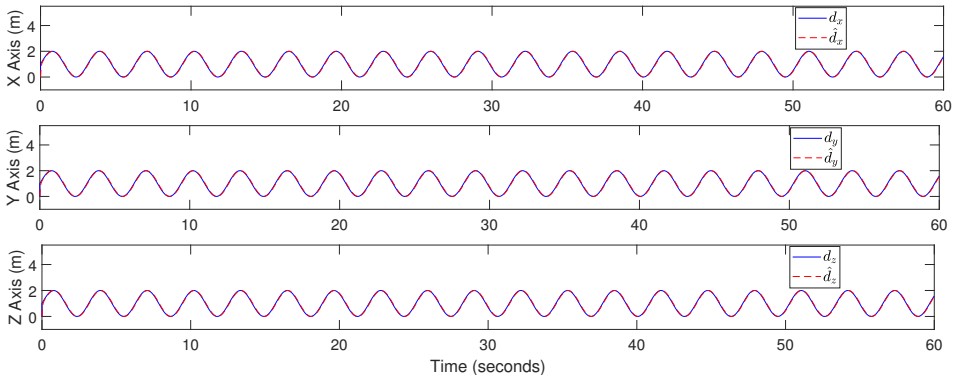

Figure 13. Disturbance observer outcome for position subsystem with periodic disturbance.

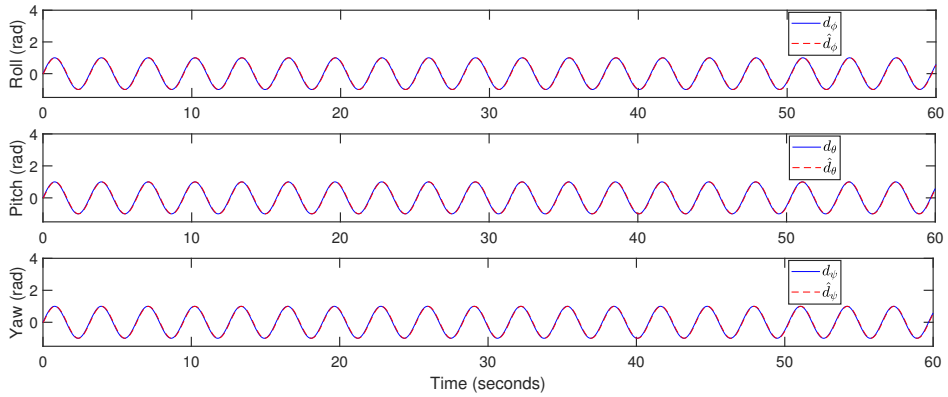

Figure 14. Disturbance observer outcome for attitude subsystem with periodic disturbance.

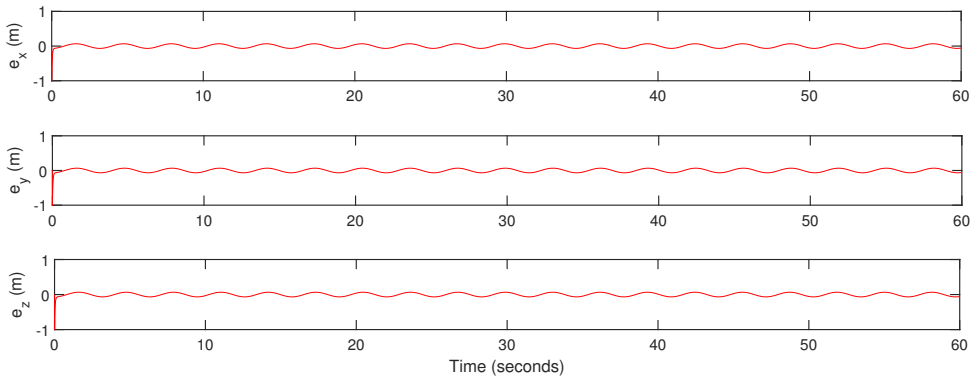

Figure 15. Estimation error of position subsystem when $[1+\sin(2t)\ 1+\sin(2t)\ 1+\sin(2t)]$ applied to position subsystem.

In Figure 16, there is a small error in the attitude subsystem. Figure 17 shows the trajectory-tracking error with observer and without observer. it can be seen that there are small (0.05 m) steady-state errors in the z axis during takeoff and landing and during hovering mode there is no error. Tracking error with observer in x-y axis is much better then without observer, which validates the designed nonlinear observer's performance with periodic disturbance and from Figure 18 it can be seen that there is a very small tracking error of attitude subsystem when periodic disturbance is applied.

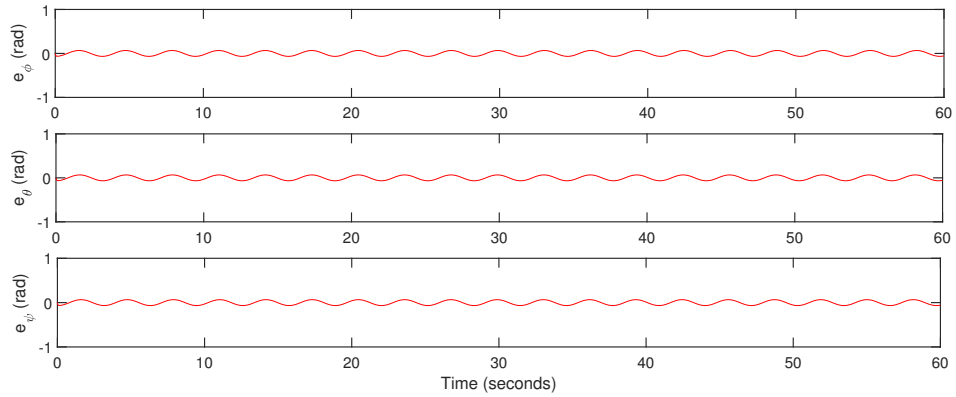

Figure 16. Estimation error of attitude subsystem when $[\sin(2t)\ \ \sin(2t)\ \ \sin(2t)]$ is applied to the attitude subsystem.

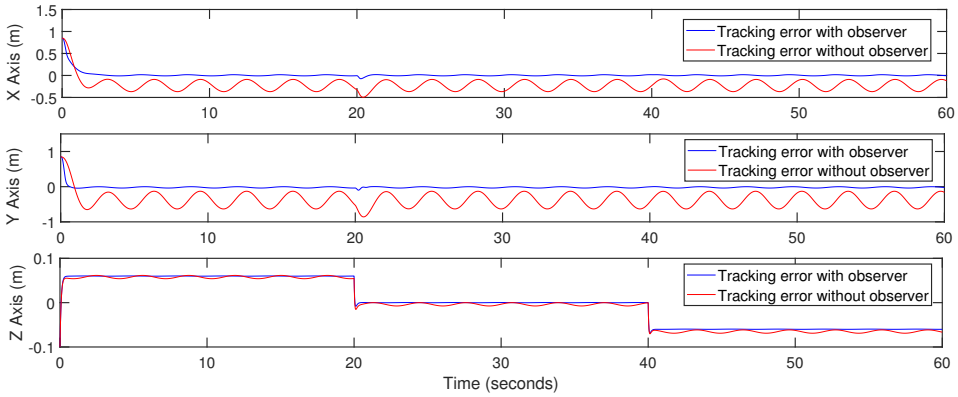

Figure 17. Position tracking Error when $[1 + \sin(2t)\ 1 + \sin(2t)\ 1 + \sin(2t)]$ is applied to the attitude subsystem.

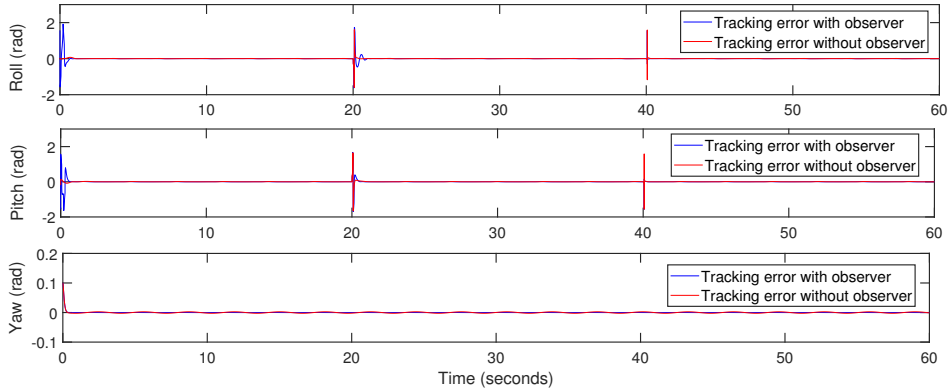

Figure 18. Attitude tracking error when $[\sin(2t)\ \sin(2t)\ \sin(2t)]$ is applied to the attitude subsystem.

Next, we apply the Von Karman wind gust model (turbulence model) as an external disturbance. External disturbances such as wind gusts have more impact in the takeoff, landing hovering mode in actual scenarios. We present simulation work for the takeoff, landing and hovering phase with a Von Karman turbulence model that evaluates the proposed nonlinear controller's performance. Figure 19 shows the position tracking with wind gust, providing small changes in the positioning subsystem during takeoff, landing and hovering.

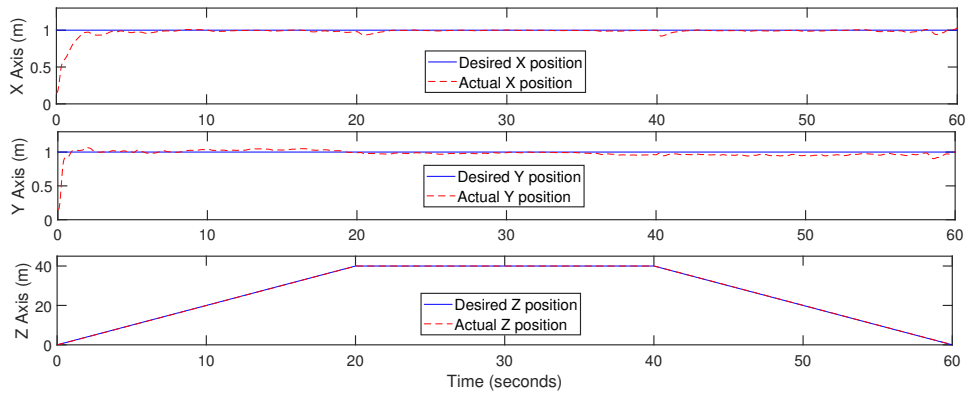

Figure 19. Position tracking with Von Karman wind turbulence model.

Similarly, Figure 20 shows small fluctuations in the attitude subsystem.

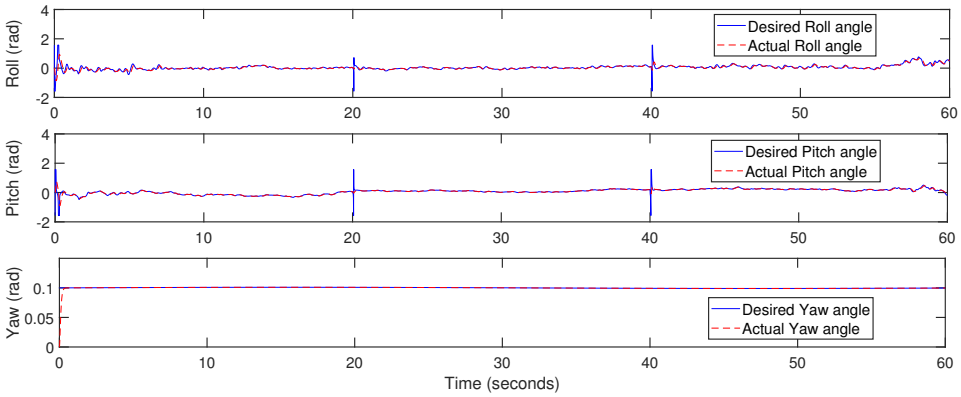

Figure 20. Attitude tracking with Von Karman wind turbulence model.

Figures 21 and 22 show the observer's performance during estimation of disturbance. These results validate the designed nonlinear observer's performance.

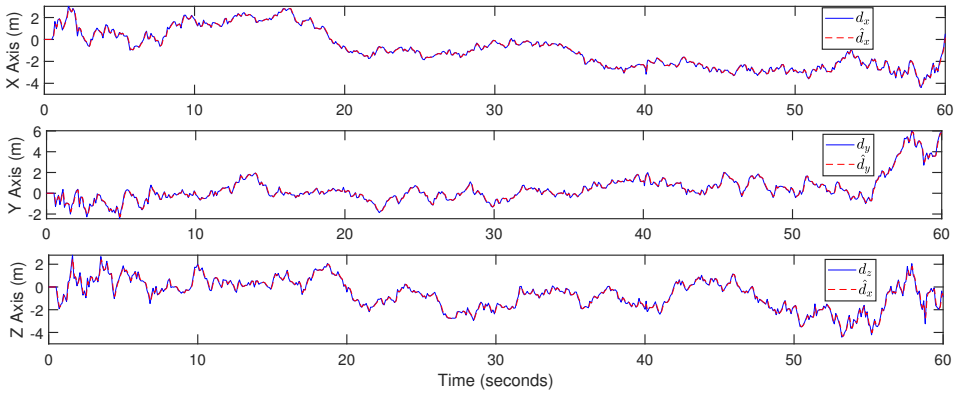

Figure 21. Disturbance observer outcome for position subsystem with Von Karman wind turbulence model.

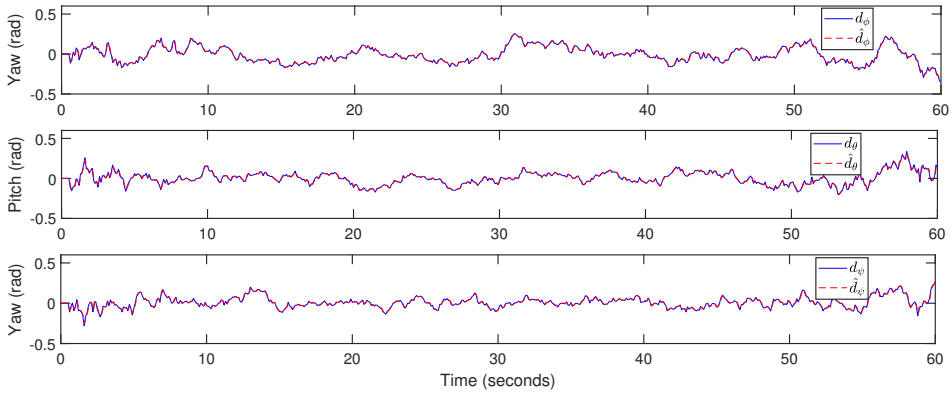

Figure 22. Disturbance observer outcome for attitude subsystem with Von Karman wind turbulence model.

Figures 23 and 24 show the performance of disturbance observer for position and attitude subsystem with Von Karman wind turbulence model. It can be seen that the error is small.

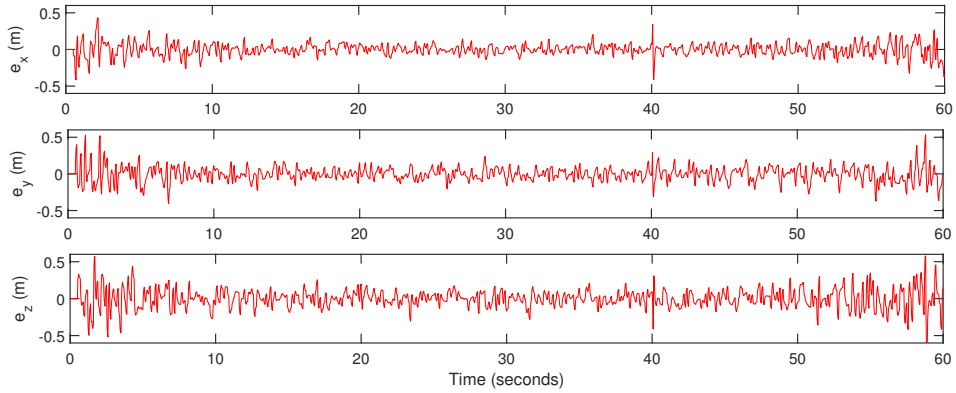

Figure 23. Estimation error of position subsystem when Von Karman wind turbulence model applied to position subsystem.

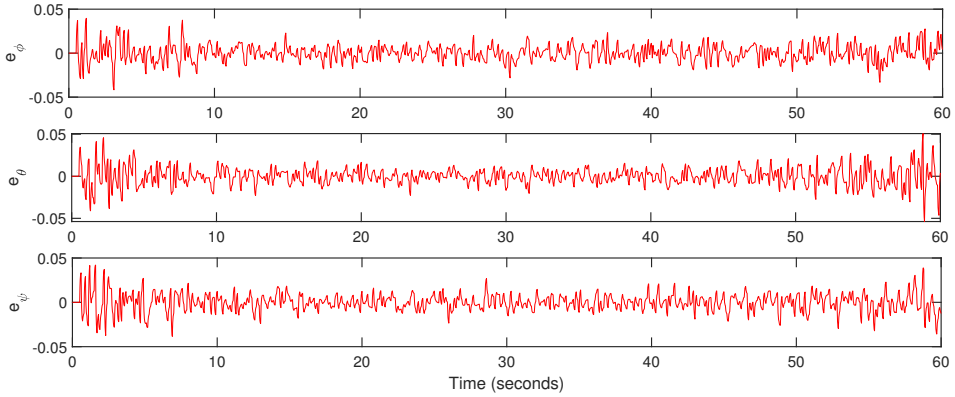

Figure 24. Estimation error of attitude subsystem when Von Karman wind turbulence model is applied to the attitude subsystem.

Figures 25 and 26 show the small tracking errors in position and attitude subsystems with and without observer where there is a small (0.05 m) steady-state error in the z-axis during takeoff and landing, with wind gust applied.

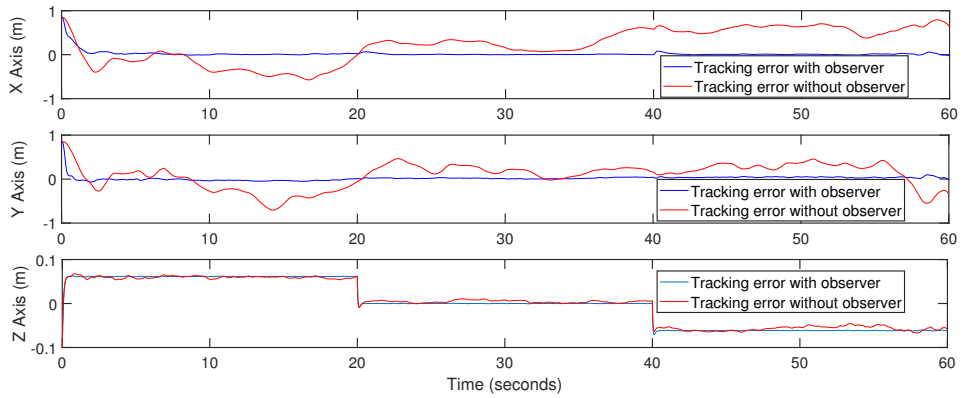

Figure 25. Position tracking error when Von Karman wind turbulence model is applied to the attitude subsystem.

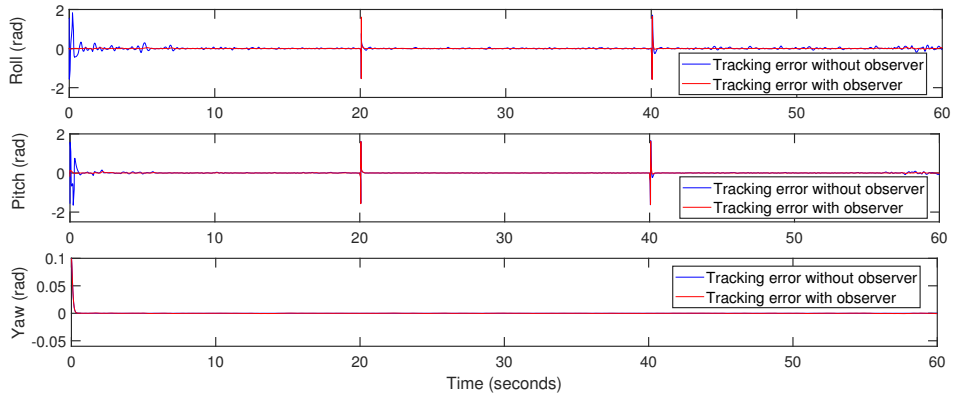

Figure 26. Attitude tracking error when Von Karman wind turbulence model is applied to the attitude subsystem.

Figure 27 shows the comparison between nonlinear observer-based backstepping controller (NDO-BC) and nominal backstepping Controller (BC) when periodic disturbance and wind gust acting on tail-sitter while tracking trajectory $[1 + \sin(0.5t)\ 1 + \cos(0.5t)\ 2t]$ in quadrotor mode. It can be seen that nonlinear observer-based backstepping controller performance is far better then the nominal backstepping controller.

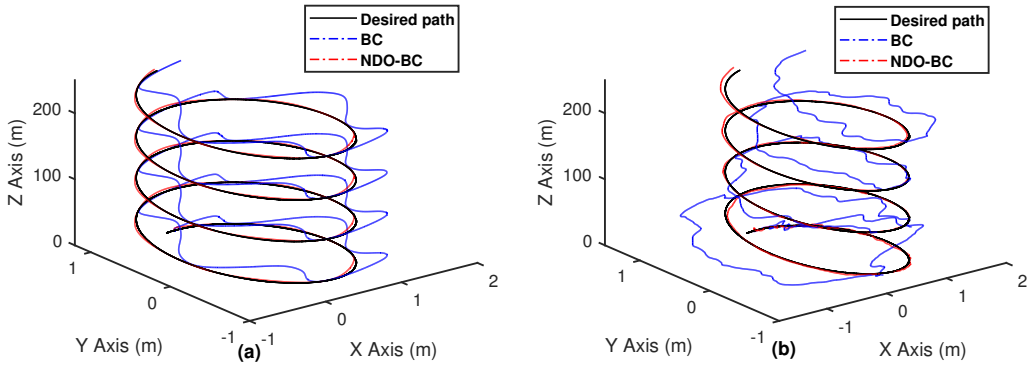

Figure 27. Comparison of nonlinear disturbance observer-based backstepping controller and nominal backstepping controller when (**a**) periodic disturbance (**b**) wind gust applied in Quadrotor Mode.

6. Conclusions

In this paper, a backstepping controller is designed for quadrotor tail-sitter UAVs for an autonomous flight with takeoff, hovering mode, level-flight mode, and landing phase. The nonlinear disturbance is designed to estimate external disturbance for hovering mode. Three different types of external disturbance are applied. The Von Karman wind gust model is applied as an external disturbance during the landing and takeoff phase. We formulated an appropriate dynamical model considering wind gust disturbances in MATLAB/Simulink and carried out simulation work. Simulation results show that the presented backstepping controller effectively controls all phases of autonomous flight. During transition maneuver, there is negligible altitude drop and successfully tracking of the commanded trajectory. When different external disturbances are applied to the UAV in landing, takeoff phase, and hovering mode, it maintains its position, which demonstrates the proposed nonlinear-based backstepping controller effectiveness.

Author Contributions: Conceptualization, N.D. and D.D.; methodology, D.D. and N.D.; software, N.D.; validation, N.D.; formal analysis, D.D.; writing—original draft preparation, N.D. and M.K.; writing—review and editing, D.D., M.K. and S.O.; supervision, D.D.; funding acquisition, S.O. All authors have read and agreed to the published version of the manuscript.

Funding: This research was funded by the European Regional Development Fund in the Research Centre of Advanced Mechatronic Systems project, within the Operational Programme Research, Development and Education, grant number: *CZ*.02.1.01/0.0/0.0/16_019/0000867.

Institutional Review Board Statement: Not Applicable.

Informed Consent Statement: Not Applicable.

Conflicts of Interest: The authors declare no conflict of interest.

References

1. Kita, K.; Konno, A.; Uchiyama, M. Transition between Level Flight and Hovering of a Tail-Sitter Vertical Takeoff and Landing Aerial Robot. *Adv. Robot.* **2010**, *24*, 763–781. [CrossRef]
2. Zhang, F.; Lyu, X.; Wang, Y.; Gu, H.; Li, Z. Modeling and Flight Control Simulation of a Quadrotor Tailsitter VTOL UAV. In Proceedings of the AIAA Modeling and Simulation Technologies Conference, Grapevine, TX, USA, 9–13 January 2017; American Institute of Aeronautics and Astronautics: Reston, VA, USA, 2017. [CrossRef]
3. Bapst, R.; Ritz, R.; Meier, L.; Pollefeys, M. Design and implementation of an unmanned tail-sitter. In Proceedings of the 2015 IEEE/RSJ International Conference on Intelligent Robots and Systems (IROS), Hamburg, Germany, 28 September–3 October 2015; IEEE: New York City, NY, USA, 2015; pp. 1885–1890.
4. Forshaw, J.L.; Lappas, V.J. Architecture and systems design of a reusable Martian twin rotor tailsitter. *Acta Astronaut.* **2012**, *80*, 166–180. [CrossRef]
5. Verling, S.; Weibel, B.; Boosfeld, M.; Alexis, K.; Burri, M.; Siegwart, R. Full Attitude Control of a VTOL tailsitter UAV. In Proceedings of the 2016 IEEE International Conference on Robotics and Automation (ICRA), Stockholm, Sweden, 16–21 May 2016; IEEE: New York City, NY, USA, 2016; pp. 3006–3012.
6. Oosedo, A.; Abiko, S.; Konno, A.; Koizumi, T.; Furui, T.; Uchiyama, M. Development of a quad rotor tail-sitter VTOL UAV without control surfaces and experimental verification. In Proceedings of the 2013 IEEE International Conference on Robotics and Automation, Karlsruhe, Germany, 6–10 May 2013; IEEE: New York City, NY, USA, 2013; pp. 317–322.
7. Oosedo, A.; Abiko, S.; Konno, A.; Uchiyama, M. Optimal transition from hovering to level-flight of a quadrotor tail-sitter UAV. *Auton. Robot.* **2016**, *41*, 1143–1159. [CrossRef]
8. Wang, Y.; Lyu, X.; Gu, H.; Shen, S.; Li, Z.; Zhang, F. Design, implementation and verification of a quadrotor tail-sitter VTOL UAV. In Proceedings of the 2017 International Conference on Unmanned Aircraft Systems (ICUAS), Miami, FL, USA, 13–16 June 2017; IEEE: New York City, NY, USA, 2017; pp. 462–471.
9. Hochstenbach, M.; Notteboom, C.; Theys, B.; Schutter, J.D. Design and Control of an Unmanned Aerial Vehicle for Autonomous Parcel Delivery with Transition from Vertical Take-off to Forward Flight – VertiKUL, a Quadcopter Tailsitter. *Int. J. Micro Air Veh.* **2015**, *7*, 395–405. [CrossRef]
10. Máthé, K.; Buşoniu, L. Vision and Control for UAVs: A Survey of General Methods and of Inexpensive Platforms for Infrastructure Inspection. *Sensors* **2015**, *15*, 14887–14916. [CrossRef] [PubMed]
11. Trotta, A.; Andreagiovanni, F.D.; Felice, M.D.; Natalizio, E.; Chowdhury, K.R. When UAVs Ride A Bus: Towards Energy-efficient City-scale Video Surveillance. In Proceedings of the IEEE INFOCOM 2018—IEEE Conference on Computer Communications, Honolulu, HI, USA, 16–19 April 2018; IEEE: New York City, NY, USA, 2018. [CrossRef]
12. Otto, A.; Agatz, N.; Campbell, J.; Golden, B.; Pesch, E. Optimization approaches for civil applications of unmanned aerial vehicles (UAVs) or aerial drones: A survey. *Networks* **2018**, *72*, 411–458. [CrossRef]
13. Chiaraviglio, L.; D'Andreagiovanni, F.; Liu, W.; Gutierrez, J.; Blefari-Melazzi, N.; Choo, K.K.R.; Alouini, M.S. Multi-Area Throughput and Energy Optimization of UAV-aided Cellular Networks Powered by Solar Panels and Grid. *IEEE Trans. Mob. Comput.* **2020**, 1. [CrossRef]
14. Li, B.; Zhou, W.; Sun, J.; Wen, C.; Chen, C. Model Predictive Control for Path Tracking of a VTOL Tailsitter UAV in an HIL Simulation Environment. In Proceedings of the 2018 AIAA Modeling and Simulation Technologies Conference, Kissimmee, FL, USA, 8–12 January 2018; American Institute of Aeronautics and Astronautics: Reston, VA, USA, 2018. [CrossRef]
15. Lyu, X.; Gu, H.; Zhou, J.; Li, Z.; Shen, S.; Zhang, F. A hierarchical control approach for a quadrotor tail-sitter VTOL UAV and experimental verification. In Proceedings of the 2017 IEEE/RSJ International Conference on Intelligent Robots and Systems (IROS), Vancouver, BC, Canada, 24–28 September 2017; IEEE: New York City, NY, USA, 2017; pp. 5135–5141.
16. Li, Z.; Zhang, L.; Liu, H.; Zuo, Z.; Liu, C. Nonlinear robust control of tail-sitter aircrafts in flight mode transitions. *Aerosp. Sci. Technol.* **2018**, *81*, 348–361. [CrossRef]
17. Zhou, H.; Xiong, H.L.; Liu, Y.; Tan, N.D.; Chen, L. Trajectory Planning Algorithm of UAV Based on System Positioning Accuracy Constraints. *Electronics* **2020**, *9*, 250. [CrossRef]
18. Flores, G.R.; Escareño, J.; Lozano, R.; Salazar, S. Quad-Tilting Rotor Convertible MAV: Modeling and Real-Time Hover Flight Control. *J. Intell. Robot. Syst.* **2011**, *65*, 457–471. [CrossRef]
19. Zhou, J.; Lyu, X.; Li, Z.; Shen, S.; Zhang, F. A unified control method for quadrotor tail-sitter UAVs in all flight modes: Hover, transition, and level flight. In Proceedings of the 2017 IEEE/RSJ International Conference on Intelligent Robots and Systems (IROS), Vancouver, BC, Canada, 24–28 September 2017; IEEE: New York City, NY, USA, 2017; pp. 4835–4841.

20. Swarnkar, S.; Parwana, H.; Kothari, M.; Abhishek, A. Biplane-Quadrotor Tail-Sitter UAV: Flight Dynamics and Control. *J. Guid. Control Dyn.* **2018**, *41*, 1049–1067. [CrossRef]
21. Flores, G.; Lugo-Cárdenas, I.; Lozano, R. A nonlinear path-following strategy for a fixed-wing MAV. In Proceedings of the 2013 International Conference on Unmanned Aircraft Systems (ICUAS), Atlanta, GA, USA, 28–31 May 2013; IEEE: New York City, NY, USA, 2013; pp. 1014–1021.
22. Brezoescu, A.; Espinoza, T.; Castillo, P.; Lozano, R. Adaptive Trajectory Following for a Fixed-Wing UAV in Presence of Crosswind. *J. Intell. Robot. Syst.* **2012**, *69*, 257–271. [CrossRef]
23. Hajiloo, A.; Rodrigues, L. Modeling and backstepping control of under-actuated spherical UAV. In Proceedings of the 2017 IEEE Conference on Control Technology and Applications (CCTA), Maui, HI, USA, 27–30 August 2017; IEEE: New York City, NY, USA, 2017; pp. 2069–2074.
24. Espinoza, T.; Dzul, A.E.; Lozano, R.; Parada, P. Backstepping—Sliding Mode Controllers Applied to a Fixed-Wing UAV. *J. Intell. Robot. Syst.* **2013**, *73*, 67–79. [CrossRef]
25. Sartori, D.; Quagliotti, F.; Rutherford, M.J.; Valavanis, K.P. Implementation and Testing of a Backstepping Controller Autopilot for Fixed-wing UAVs. *J. Intell. Robot. Syst.* **2014**, *76*, 505–525. [CrossRef]
26. Lungu, M. Auto-landing of fixed wing unmanned aerial vehicles using the backstepping control. *ISA Trans.* **2019**, *95*, 194–210. [CrossRef] [PubMed]
27. Rubí, B.; Pérez, R.; Morcego, B. A Survey of Path Following Control Strategies for UAVs Focused on Quadrotors. *J. Intell. Robot. Syst.* **2019**, *98*, 241–265. [CrossRef]
28. Lyu, X.; Zhou, J.; Gu, H.; Li, Z.; Shen, S.; Zhang, F. Disturbance Observer Based Hovering Control of Quadrotor Tail-Sitter VTOL UAVs Using Synthesis. *IEEE Robot. Autom. Lett.* **2018**, *3*, 2910–2917. [CrossRef]
29. Kikkawa, H.; Uchiyama, K. Nonlinear flight control with an extended state observer for a fixed-wing UAV. In Proceedings of the 2017 International Conference on Unmanned Aircraft Systems (ICUAS), Miami, FL, USA, 13–16 June 2017; IEEE: New York City, NY, USA, 2017. [CrossRef]
30. Guo, K.; Jia, J.; Yu, X.; Guo, L.; Xie, L. Multiple observers based anti-disturbance control for a quadrotor UAV against payload and wind disturbances. *Control Eng. Pract.* **2020**, *102*, 104560. [CrossRef]
31. Oosedo, A.; Konno, A.; Matumoto, T.; Go, K.; Masuko, K.; Abiko, S.; Uchiyama, M. Design and simulation of a quad rotor tail-sitter unmanned aerial vehicle. In Proceedings of the 2010 IEEE/SICE International Symposium on System Integration, Sendai, Japan, 21–22 December 2010; IEEE: New York City, NY, USA, 2011; pp. 254–259. [CrossRef]
32. Bouabdallah, S.; Siegwart, R. Backstepping and Sliding-mode Techniques Applied to an Indoor Micro Quadrotor. In Proceedings of the 2005 IEEE International Conference on Robotics and Automation, Barcelona, Spain, 18–22 April 2005; IEEE: New York City, NY, USA, 2006; pp. 2247–2252.
33. Chen, W.H.; Ballance, D.J.; Gawthrop, P.J.; O'Reilly, J. A nonlinear disturbance observer for robotic manipulators. *IEEE Trans. Ind. Electron.* **2000**, *47*, 932–938. [CrossRef]
34. Liu, C.; Chen, W.H.; Andrews, J. Tracking control of small-scale helicopters using explicit nonlinear MPC augmented with disturbance observers. *Control Eng. Pract.* **2012**, *20*, 258–268. [CrossRef]
35. Yang, J.; Li, S.; Yu, X. Sliding-Mode Control for Systems With Mismatched Uncertainties via a Disturbance Observer. *IEEE Trans. Ind. Electron.* **2013**, *60*, 160–169. [CrossRef]
36. Viswanath, D.; Deb, D. Disturbance Observer based Sliding Mode Control for Proportional Navigation Guidance. *IFAC Proc. Vol.* **2012**, *45*, 163–168. [CrossRef]
37. Fethalla, N.; Saad, M.; Michalska, H.; Ghommam, J. Robust Observer-Based Dynamic Sliding Mode Controller for a Quadrotor UAV. *IEEE Access* **2018**, *6*, 45846–45859. [CrossRef]
38. Patel, R.; Deb, D.; Modi, H.; Shah, S. Adaptive backstepping control scheme with integral action for quanser 2-dof helicopter. In Proceedings of the 2017 International Conference on Advances in Computing, Communications and Informatics (ICACCI), Udupi, India, 13–16 September 2017; IEEE: New York City, NY, USA, 2017. [CrossRef]
39. Patel, R.; Deb, D. Parametrized control-oriented mathematical model and adaptive backstepping control of a single chamber single population microbial fuel cell. *J. Power Sources* **2018**, *396*, 599–605. [CrossRef]
40. Patel, R.; Deb, D. Adaptive Backstepping Control of Single Chamber Microbial Fuel Cell. *IFAC-PapersOnLine* **2018**, *51*, 319–322. [CrossRef]